

# Compressing deep neural networks by matrix product operators

Ze-Feng Gao,<sup>1</sup> Song Cheng,<sup>2,3,4</sup> Rong-Qiang He,<sup>1</sup> Z. Y. Xie,<sup>1,\*</sup> Hui-Hai Zhao,<sup>5,†</sup> Zhong-Yi Lu,<sup>1,‡</sup> and Tao Xiang<sup>2,4,§</sup>

<sup>1</sup>*Department of Physics, Renmin University of China, Beijing 100872, China*

<sup>2</sup>*Institute of Physics, Chinese Academy of Sciences, Beijing 100190, China*

<sup>3</sup>*Center for Quantum Computing, Peng Cheng Laboratory, Shenzhen 518055, China*

<sup>4</sup>*University of Chinese Academy of Sciences, Beijing, 100049, China*

<sup>5</sup>*RIKEN Brain Science Institute, Hirosawa, Wako-shi, Saitama, 351-0106, Japan*

A deep neural network is a parametrization of a multilayer mapping of signals in terms of many alternatively arranged linear and nonlinear transformations. The linear transformations, which are generally used in the fully connected as well as convolutional layers, contain most of the variational parameters that are trained and stored. Compressing a deep neural network to reduce its number of variational parameters but not its prediction power is an important but challenging problem toward the establishment of an optimized scheme in training efficiently these parameters and in lowering the risk of overfitting. Here we show that this problem can be effectively solved by representing linear transformations with matrix product operators (MPOs), which is a tensor network originally proposed in physics to characterize the short-range entanglement in one-dimensional quantum states. We have tested this approach in five typical neural networks, including FC2, LeNet-5, VGG, ResNet, and DenseNet on two widely used data sets, namely, MNIST and CIFAR-10, and found that this MPO representation indeed sets up a faithful and efficient mapping between input and output signals, which can keep or even improve the prediction accuracy with a dramatically reduced number of parameters. Our method greatly simplifies the representations in deep learning, and opens a possible route toward establishing a framework of modern neural networks which might be simpler and cheaper, but more efficient.

## I. Introduction

Deep neural networks<sup>1-11</sup> are important tools of artificial intelligence. Their applications in many computing tasks, for example, in the famous ImageNet Large Scale Visual Recognition Challenge (ILSVRC)<sup>12</sup>, large vocabulary continuous speech recognition<sup>13</sup>, and natural language processing<sup>14</sup>, have achieved great success. They have become the most popular and dominant machine-learning approaches<sup>15</sup> that are used in almost all recognition and detection tasks<sup>16?</sup>, including but not limited to, language translation<sup>17</sup>, sentiment analysis<sup>18</sup>, segmentation and reconstruction<sup>19</sup>, drug activity prediction<sup>20</sup>, feature identification in big data<sup>21</sup>, and have attracted increasing attention from almost all natural science and engineering communities, including mathematics<sup>22,23</sup>, physics<sup>24-28</sup>, biology<sup>19,29</sup>, and materials science<sup>30</sup>.

A deep feedforward neural network sets up a mapping between a set of input signals, such as images, and a set of output signals, say categories, through a multilayer transformation,  $\mathcal{F}$ , which is represented as a composition of many alternatively arranged linear ( $\mathcal{L}$ ) and nonlinear ( $\mathcal{N}$ ) mappings<sup>31,32</sup>. More specifically, an  $n$ -layer neural network  $\mathcal{F}$  is a sequential product of alternating linear and nonlinear transformations:

$$\mathcal{F} = \mathcal{N}_n \mathcal{L}_n \cdots \mathcal{N}_2 \mathcal{L}_2 \mathcal{N}_1 \mathcal{L}_1. \quad (1)$$

The linear mappings contain most of the variational parameters that need to be determined. The nonlinear mappings, which contain almost no free parameters, are realized by some operations known as activations, including rectified linear unit, softmax, and so on.

A linear layer maps an input vector  $\mathbf{x}$  of dimension  $N_x$  to an output vector  $\mathbf{y}$  of dimension  $N_y$  via a linear transformation characterized by a weight matrix  $W$ :

$$\mathbf{y} = W\mathbf{x} + \mathbf{b}. \quad (2)$$

A fully connected layer plays the role as a global linear transformation, in which each output element is a weighted summation of all input elements, and  $W$  is a full matrix. A convolutional layer<sup>2</sup> represents a local linear transformation, in the sense that each element in the output is a weighted summation of a small portion of the elements, which form a local cluster, in the input. The variational weights of this local cluster form a dense convolutional kernel, which is designated to extract some specific features. To maintain good performance, different kernels are used to extract different features. A graphical representation of  $W$  is shown in Fig. 1(a).

Usually, the number of elements or neurons,  $N_x$  and  $N_y$ , are very large, and thus there are a huge number of parameters to be determined in a fully connected layer<sup>9</sup>. The convolutional layer reduces the variational parameters by grouping the input elements into many partially overlapped kernels, and one output element is connected to one kernel. The number of variational parameters in a convolutional layer is determined by the number of kernels and the size of each kernel. It could be much less than that in a fully connected layer. However, the total number of parameters in all the convolutional layers can still be very large in a deep neural network which contains many convolutional layers<sup>10</sup>. To train and store these parameters raises a big challenge in this field. First, it is time consuming to train and optimize these parameters, and may even increase the probability of overfitting. This would limit the generalization power of deep neural networks. Second, it needs a big memory space to store these parameters. This would limit its applications where the space of hard disk is strongly confined; for example, on mobile terminals.

There are similar situations in the context of quantum information and condensed-matter physics. In a quantum many-body system, the Hamiltonian or any other physical operator can be expressed as a higher-order tensor in the space spanned by the local basis states<sup>33</sup>. To represent exactly a

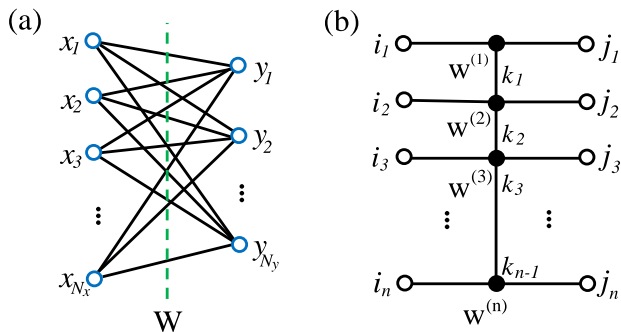


FIG. 1. (a) Graphical representation of the weight matrix  $W$  in a fully connected layer. The blue circles represent neurons, e.g., pixels. The solid line connecting an input neuron  $x_i$  with output neuron  $y_j$  represents the weight element  $W_{ji}$ . (b) MPO factorization of the weight matrix  $W$ . The local operators  $w^{(k)}$  are represented by filled circles. The hollow circles denote the input and output indices,  $i_l$  and  $j_l$ , respectively. Given  $i_k$  and  $j_k$ ,  $w^{(k)}[j_k, i_k]$  is a matrix.

quantum many-body system, the total number of parameters that need to be introduced can be extremely huge, and should in principle grow exponentially with the system size (or the size of each “image” in the language of neural network). The matrix product operator (MPO) was originally proposed in physics to characterize the short-range entanglement in one-dimensional quantum systems<sup>34,35</sup>, and is now a commonly used approach to represent effectively a higher-order tensor or Hamiltonian with short-range interactions. Mathematically, it is simply a tensor-train approximation<sup>36,37</sup> that is used to factorize a higher-order tensor into a sequential product of the so-called local tensors. Using the MPO representation, the number of variational parameters needed is greatly reduced since the number of parameters contained in an MPO just grows linearly with the system size. Nevertheless, it turns out that to provide an efficient and faithful representation of the systems with short-range interactions whose entanglement entropies are upper bounded<sup>38,39</sup> or, equivalently, the systems with finite excitation gaps in the ground states. The application of MPOs in condensed-matter physics and quantum information science has achieved great successes<sup>40,41</sup> in the past decade.

In this paper, we propose to solve the parameter problem in neural networks by employing the MPO representation, which is illustrated in Fig. 1(b) and expressed in Eq. (5). The starting point is the observation that the linear transformations in a commonly used deep neural network have a number of similar features as the quantum operators, which may allow us to simplify their representations. In a fully connected layer, for example, it is well known that the rank of the weight matrix is strongly restricted<sup>42–44</sup>, due to short-range correlations or entanglements among the input pixels. This suggests that we can safely use a lower-rank matrix to represent this layer without affecting its prediction power. In a convolutional layer, the correlations of images are embedded in the kernels, whose sizes are generally very small in comparison with the whole image size. This implies that the “extracted features” from this convolution can be obtained from very local clusters. In

both cases, a dense weight matrix is not absolutely necessary to perform a faithful linear transformation. This peculiar feature of linear transformations results from the fact that the information hidden in a data set is just short-range correlated. Thus, to accurately reveal the intrinsic features of a data set, it is sufficient to use a simplified representation that catches more accurately the key features of local correlations. This motivates us to adopt MPOs to represent linear transformation matrices in deep neural networks.

There have been several applications of tensor network structures in neural networks<sup>37,45–50</sup>. Our approach differs from them by the following aspects: (1) It is physically motivated, emphasizes more on the local structure of the relevant information, and helps to understand the success of deep neural networks. (2) It works in the framework of neural networks, in the sense that the multiple-layer structure and activation functions are still retained, and the parameters are entirely optimized through algorithms developed in neural networks. (3) It is a one-dimensional representation, and is flexible to represent the linear transformations including both the fully-connected layers and the entire convolutional layers. (4) It is also used to characterize the complexity of image datasets; (5) A systematic study has been done. These issues will become clear in the following sections.

The rest of the paper is structured as follows. In Sec. II, we present the way the linear layers can be represented by MPO and the training algorithm of the resulting network. In Sec. III, we apply our method systematically to five main neural networks, including FC2, LeNet-5, VGG, ResNet, and DenseNet on two widely used data sets, namely, MNIST and CIFAR-10. Experiments on more data sets can be found in Sec. II A in the supplemental materials<sup>51</sup> (SM). Finally, in Sec. IV, we discuss the relation with previous efforts, and the possibility to construct a framework of neural networks based on the matrix product representations in the future. In the SM<sup>51</sup>, we give the detailed structure of the neural networks used in this work, and provide extra information details about the MPO representations.

## II. Method

In this paper, the weight matrices  $W$  appearing in Eq. (2) and representing linear mappings in the most parameter-consuming layers, to be precise, all the fully connected layers and some of the heaviest convolutional layers are expressed as MPOs. To construct the MPO representation of a weight matrix  $W$ , we first reshape it into a  $2n$ -indexed tensor:

$$W_{yx} = W_{j_1 j_2 \dots j_n, i_1 i_2 \dots i_n}. \quad (3)$$

Here, the one-dimensional coordinate  $x$  of the input signal  $\mathbf{x}$  with dimension  $N_x$  is reshaped into a coordinate in an  $n$ -dimensional space, labeled  $(i_1 i_2 \dots i_n)$ . Hence, there is a one-to-one mapping between  $x$  and  $(i_1 i_2 \dots i_n)$ . Similarly, the one-dimensional coordinate  $y$  of the output signal  $\mathbf{y}$  with dimension  $N_y$  is also reshaped into a coordinate in an  $n$ -dimensional space, and there is a one-to-one correspondence between  $y$

and  $(j_1, j_2, \dots, j_n)$ . If  $I_k$  and  $J_k$  are the dimensions of  $i_k$  and  $j_k$ , respectively, then

$$\prod_{k=1}^n I_k = N_x, \quad \prod_{k=1}^n J_k = N_y. \quad (4)$$

The index decomposition in Eq. (3) is not unique. One should in principle decompose the input and output vectors such that the test accuracy is the highest. However, to test all possible decompositions is time consuming. For the results presented in this paper, we have done the decomposition just by convenience, i.e., simply reshaping the single dimension  $N_x$  as  $n$  parts  $\{I_1, I_2, \dots, I_n\}$  in order. In fact, it can be argued and verified by examples that when the network is away from underfitting, different factorization manners should always produce almost the same result. More details can be found in Sec. II B in the SM<sup>51</sup>.

The MPO representation of  $W$  is obtained by factorizing it into a product of  $n$  local tensors,

$$W_{j_1 \dots j_n, i_1 \dots i_n} = \text{Tr} \left( w^{(1)}[j_1, i_1] w^{(2)}[j_2, i_2] \cdots w^{(n)}[j_n, i_n], \right) \quad (5)$$

where  $w^{(k)}[j_k, i_k]$  is a  $D_{k-1} \times D_k$  matrix with  $D_k$  the dimension of the bond linking  $w^{(k)}$  and  $w^{(k+1)}$ . In this case,  $D_0 = D_n = 1$ . For convenience in the discussion below, we assume  $D_k = D$  for all  $k$  except  $k = 0$  or  $n$ . A graphical representation of this MPO is shown in Fig. 1(b).

In this MPO representation, the tensor elements of  $w^{(k)}$  are variational parameters. The number of parameters increases with the increase of the bond dimension  $D$ . Hence  $D$  serves as a tunable parameter that controls the expressive power. In quantum many-body systems,  $D$  also controls the expressive accuracy of a target state variationally.

The tensor elements of  $w^{(k)}$  in Eq. (5), instead of the elements of  $W$  in Eq. (2), are the variational parameters that need to be determined in the training procedure of deep neural networks. For an MPO whose structure is defined by Eq. (8), the total number of these variational parameters equals

$$N_{\text{mpo}} = \sum_{k=2}^{n-1} I_k J_k D^2 + I_1 J_1 D + I_n J_n D, \quad (6)$$

which will be a great reduction of the number  $N_x N_y$  in the original fully connected layers (when  $N_x$  and  $N_y$  are large) and of the number  $N_k N_0$  in the original convolutional layers (when the kernel size  $N_0$  and the number of kernels  $N_k$  are large).

The strategy of training is to find a set of optimal  $w$ 's so the following cost function is minimized,

$$L = - \sum_m \sum_i t_m^T \log y_m + \frac{\alpha}{2} \sum_i |w^{(i)}|^2, \quad (7)$$

where  $m$  is the label of images,  $i$  is the label of all the parameters, including the local tensors in the MPO representations and the kernels in the untouched convolutional layers.  $|w|$  represents the norm of parameter  $w$ , and  $\alpha$  is an empirical parameter that is fixed prior to the training. The first term measures

the cross entropy between prediction vectors  $y$  and target label vectors  $t$ . The second term is a constraint, called the L2 regularization<sup>52</sup>, which is a widely adopted technique in deep learning to alleviate overfitting, and thus it is also used in all the networks mentioned in this paper, including both the normal neural networks, such as FC2, LeNet-5, VGG, ResNet, as well as DenseNet, and the corresponding MPO-Net counterparts. It should be mentioned that the usage of the L2 regularization has little to do with the validity of the MPO representations, i.e., without L2 regularization, the MPO-Nets should still work as well as the normal networks, as shown in Sec. II D in the SM<sup>51</sup>.

To implement a training step,  $L$  is evaluated using the known  $w$ 's, which are randomly initialized, and the input data set. The gradients of the cost function with respect to the variational parameters are determined by the standard back propagation<sup>53</sup>. All the parameters  $w$  are treated equally and are updated by the stochastic gradient descent with momentum algorithm<sup>54</sup> in parallel. This is different from the previous effort<sup>37</sup> and is more suitable for deep learning. This training step is terminated when the cost function stops to drop.

The detailed structures of the neural networks we have studied, as well as the performance on more datasets, different factorization manners, entanglement entropy grasped, the influence of L2 regularization, convergence of training, and so on, are appended systematically in the SM<sup>51</sup>. The specific setting of the hyper-parameters for training can be found in the source code<sup>55</sup>.

### III. Results

Here we show the results obtained with the MPO representation in five kinds of typical neural networks on two datasets, i.e., FC2<sup>56</sup> and LeNet-5<sup>2</sup> on the MNIST data set<sup>57</sup>; VGG<sup>9</sup>, ResNet<sup>10</sup>, and DenseNet<sup>11</sup> on the CIFAR-10 data set<sup>58</sup>. Among them, FC2 and LeNet-5 are relatively shallow in the depth of network, while VGG, Residual CNN (ResNet), and Dense CNN (DenseNet) are deeper neural networks.

For convenience, we use MPO-Net to represent a deep neural network with all or partial linear layers being represented by MPOs. Moreover, we denote an MPO, defined by Eq. (5), as

$$M_{I_1, I_2, \dots, I_n}^{J_1, J_2, \dots, J_n}(D). \quad (8)$$

To quantify the compressibility of MPO-net with respect to a neural network, we define its compression ratio  $\rho$  as

$$\rho = \frac{\sum_l N_{\text{mpo}}^{(l)}}{\sum_l N_{\text{ori}}^{(l)}}, \quad (9)$$

where  $\sum_l$  is to sum over the linear layers whose transformation tensors are replaced by MPO.  $N_{\text{ori}}^{(l)}$  and  $N_{\text{mpo}}^{(l)}$  are the number of parameters in the  $l$ -th layer in the original and MPO representations, respectively. The smaller is the compression ratio, the fewer number of parameters is used in the MPO representation.

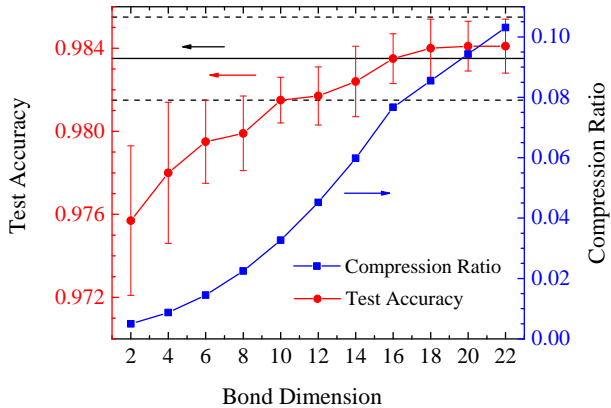


FIG. 2. Performance of the MPO representations in FC2 on MNIST. The solid straight line denotes the test accuracy obtained by the normal FC2,  $98.35\% \pm 0.2\%$ , and the dashed straight lines are plotted to indicate its error bar.

Furthermore, to examine the performance of a given neural network, we train the network  $m$  times independently to obtain a test accuracy  $a$  with a standard deviation  $\sigma$  defined by

$$a = \bar{a} \pm \sigma, \quad (10)$$

$$\sigma = \frac{1}{\sqrt{m-1}} \left[ \sum_{i=1}^m (a_i - \bar{a})^2 \right]^{1/2}, \quad (11)$$

where  $a_i$  is the test accuracy of the  $i$ -th training procedure.  $\bar{a}$  is the average of  $\{a_i\}$ . The results presented in this paper are obtained with  $m = 5$ .

### A. MNIST dataset

We start from the identification of handwritten digits in the MNIST dataset<sup>57</sup>, which consists of 60000 digits for training and 10000 digits for testing. Each image is a square of  $28 \times 28$  grayscale pixels, and all the images are divided into ten classes corresponding to numbers 0 ~ 9, respectively.

#### 1. FC2

We first test the MPO representation in the simplest textbook structure of neural network, i.e., FC2<sup>56</sup>. FC2 consists of only two fully connected layers whose weight matrices have  $784 \times 256$  and  $256 \times 10$  elements, respectively. We replace these two weight matrices, respectively, by  $M_{4,7,7,4}^{4,4,4,4}(D)$  and  $M_{4,4,4,4}^{1,1,10,1}(4)$  in the corresponding MPO representation. Here we fix the bond dimension in the second layer to 4, and only allow the bond dimension to vary in the first layer.

Figure 2 compares the results obtained with FC2 and the corresponding MPO-Net. The test accuracy of MPO-Net increases when the bond dimension  $D$  is increased. It reaches

TABLE I. Test accuracy  $a$  and compression ratios  $\rho$  obtained in the original and MPO representations of LeNet-5 on MNIST and VGG on CIFAR-10.

Data set	Network	Original Rep	MPO-Net	
		$a$ (%)	$a$ (%)	$\rho$
MNIST	LeNet-5	$99.17 \pm 0.04$	$99.17 \pm 0.08$	0.05
CIFAR-10	VGG-16	$93.13 \pm 0.39$	$93.76 \pm 0.16$	$\sim 0.0005$
	VGG-19	$93.36 \pm 0.26$	$93.80 \pm 0.09$	$\sim 0.0005$

the accuracy of the normal FC2 when  $D = 16$ . Even for the  $D = 2$  MPO-Net, which has only 1024 parameters, about 200 times less than the original FC2, the test accuracy is already very good. This shows that the linear transformations in FC2 are very local and can indeed be effectively represented by MPOs. The compression ratio of MPO-Net decreases with increasing  $D$ . But even for  $D = 16$ , the compression ratio is still below 8%, which indicates that the number of parameters to be trained can be significantly reduced without any accuracy loss.

#### 2. LeNet-5

We further test MPO-Net with the famous LeNet-5 network<sup>2</sup>, which is the first instance of convolutional neural networks. LeNet-5 has five linear layers. Among them, the last convolutional layer and the two fully connected layers contain the most of parameters. We represent these three layers by three MPOs, which are structured as  $M_{2,10,10,2}^{2,5,6,2}(4)$ ,  $M_{2,5,6,2}^{2,3,7,2}(4)$ , and  $M_{2,3,7,2}^{1,5,2,1}(2)$ , respectively. The compression ratio is  $\rho \sim 0.05$ .

Table I shows the results obtained with the original and MPO representations of LeNet-5. We find that the test accuracy of LeNet-5 can be faithfully reproduced by MPO-Net. Since LeNet-5 is the first and prototypical convolutional neural network, this success gives us confidence in using the MPO presentation in deeper neural networks.

### B. CIFAR-10 dataset

CIFAR-10 is a more complex dataset<sup>58</sup>. It consists of 50000 images for training and 10000 images for testing. Each image is a square of  $32 \times 32$  RGB pixels. All the images in this data set are divided into ten classes corresponding to airplane, automobile, ship, truck, bird, cat, deer, dog, frog, and horse, respectively. To have a good classification accuracy, deeper neural networks with many convolutional layers are used. To show the effectiveness of MPOs representation, as a preliminary test, we use MPO only on the fully connected layers and on some heavily parameter-consuming convolutional layers.

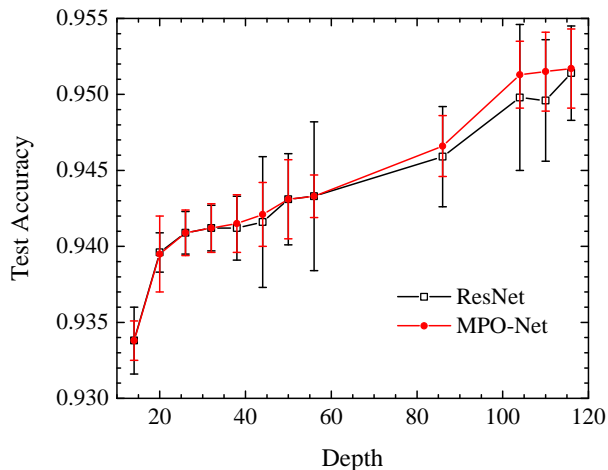


FIG. 3. Comparison of the test accuracy  $a$  between the original and MPO representations of ResNet on CIFAR-10 with  $k = 4$ . The compression ratio of MPO-Net  $\rho \sim 0.11$ .

### 1. VGG

VGG<sup>9</sup> is the first *very* deep neural network constructed. It won first place in the localization task of the ILSVRC competition 2014. We have tested two well-established VGG structures, which have 16 and 19 layers, respectively. In both cases, there are many convolutional layers and three fully connected layers. We represent the last two heaviest convolutional layers and all the three fully connected layers, respectively, by MPO with the structures:  $M_{2,8,8,8,2}^{2,8,8,8,2}(4)$ ,  $M_{2,8,8,8,2}^{2,8,8,8,2}(4)$ ,  $M_{4,4,8,8,4}^{4,4,8,8,4}(4)$ ,  $M_{4,4,8,8,4}^{4,4,8,8,4}(4)$ , and  $M_{4,4,8,8,4}^{1,10,1,1,1}(4)$ . The result is summarized in Table I.

For both structures, the compression ratio of MPO-Net is about 0.0005. Hence the number of parameters used is much less than in the original representation. However, we find that the prediction accuracy of MPO-Net is even better than those obtained from the original networks. This is consistent with the results reported by Novikov<sup>37</sup> for the ImageNet data set<sup>59</sup>. It results from two facts of MPOs: First, since the number of variational parameters is greatly reduced in MPO-Net, the representation is more economical and it is easier to train the parameters. Second, the local correlations between input and output elements are more accurately represented by MPO. This can reduce the probability of overfitting.

### 2. ResNet

ResNet<sup>10</sup> is commonly used to address the degradation problem with deep convolutional neural networks. It won first place on the detection task in ILSVRC in 2015, and differs from the ordinary convolutional neural network by the so-called ResUnit structure, in which identity mappings are added to connect some of the input and output signals. The ResNet structure used in our calculation has a fully connected layer realized by a weight matrix of  $64k \times 10$ . Here  $k$  con-

trols the width of the network. We represent this layer by an MPO of  $M_{4,4,4,k}^{1,5,2,1}(3)$ . In our calculation,  $k = 4$  is used and the corresponding compression ratio is about 0.11.

Figure 3 shows the test accuracy as a function of the depth of layers of ResNet with  $k = 4$ . We find that MPO-Net has the same accuracy as the normal ResNet for all the cases we have studied. We also find that even the ResUnit can be compressed by MPO. For example, for the 56-layer ResNet, by representing the last heaviest ResUnit and the fully connected layer with two  $M_{2,4,4,4,4,4,2}^{2,4,4,4,4,4,2}(4)$  and one  $M_{4,4,4,k}^{1,5,2,1}(3)$ , we obtain the same accuracy as the normal ResNet. Similar observations are obtained for other  $k$  values.

### 3. DenseNet

The last deep neural network we have tested is DenseNet<sup>11</sup>. Constructed in the framework of ResNet, DenseNet modifies ResUnit to DenseUnit by adding more shortcuts in the units. This forms a wider neural network, allowing the extracted information to be more efficiently recycled. It also achieved great success in the ILSVRC competition, and drew much attention in the CVPR conference in 2017.

The DenseNet used in this work has a fully connected layer with a weight matrix of  $(n + 3km) \times 10$ , where  $m$  controls the total depth  $L$  of the network,  $L = 3m + 4$ ,  $n$  and  $k$  are the other two parameters that specify the network. There is only one fully connected layer in DenseNet, and we use MPO to reduce the parameter number in this layer. Corresponding to different  $m$ ,  $k$ , and  $n$ , we use different MPO representations.

Our results are summarized in Table II. For the four DenseNet structures we have studied, the fully connected layer is compressed by more than seven to 21 times. The corresponding compression ratios vary from 0.044 to 0.129. In the first three cases, we find that the test precisions obtained with MPO-Net agree with the DenseNet results within numerical errors. For the fourth case, the test accuracy obtained with MPO-Net is even slightly higher than that obtained with DenseNet. Furthermore, in the first structure listed in Table II, we have also tried to replace the last heaviest convolutional layer by  $M_{4,5,8,11,4,4}^{2,4,4,3,4,2}(20)$  while keeping the last fully connected layer represented by  $M_{4,4,7,4}^{1,5,2,1}(4)$ . The obtained accuracy is about  $93.52 \pm 0.40$ , which is still consistent with the original DenseNet result  $93.56 \pm 0.26$ . The corresponding compression ratio is also considerable, i.e.,  $\rho \sim 0.497$ .

Applications to more data sets, such as the Fashion-MNIST<sup>60</sup> and Street View House Number data sets<sup>61</sup>, can be found in Sec. II A in the SM<sup>51</sup>. We found that the faithful representation and the effective compression capability of MPO are also valid there.

## IV. Discussion

Motivated by the success of MPOs in the study of quantum many-body systems with short-range interactions, we propose to use MPOs to represent linear transformation matrices in deep neural networks. This is based on the assumption that

TABLE II. Performance of MPO representations in DenseNet on CIFAR-10.

Depth	(n, m, k)	Test accuracy (%)		MPO structure	$\rho$
		DenseNet	MPO-Net		
40	(16, 12, 12)	93.56 $\pm$ 0.26	93.59 $\pm$ 0.13	$M_{4,4,7,4}^{1,5,2,1}(4)$	0.129
40	(16, 12, 24)	95.12 $\pm$ 0.15	95.13 $\pm$ 0.13	$M_{4,5,11,4}^{1,5,2,1}(4)$	0.089
100	(24, 32, 12)	95.36 $\pm$ 0.15	95.58 $\pm$ 0.07	$M_{4,7,7,6}^{1,5,2,1}(4)$	0.070
100	(96, 32, 24)	95.74 $\pm$ 0.09	96.09 $\pm$ 0.07	$M_{5,8,12,5}^{1,5,2,1}(4)$	0.044

the correlations between pixels, or the inherent structures of information hidden in “images”, are essentially localized<sup>62,63</sup>, which enables us to make an analogy between an image and a quantum state and further between a linear mapping in neural network and a quantum operator in physics. We have tested our approach with five different kinds of typical neural networks on two data sets, and found that MPOs can not only improve the efficiency in training and reduce the memory space, as originally expected, but also slightly improve the test accuracy using much fewer number of parameters than in the original networks. This, as already mentioned, may result from the fact that the variational parameters can be more accurately and efficiently trained due to the dramatic reduction of parameters in MPO-Net. The MPO representation emphasizes more on the local correlations of input signals. It puts a strong constraint on the linear transformation matrix and avoids the training data being trapped at certain local minima. We believe this can reduce the risk of overfitting.

In fact, by using the canonical form<sup>64</sup> of an MPO representation obtained from training, we can introduce the entanglement entropy, initially defined for a quantum state in physics, for a dataset in deep learning to quantify the expressive ability of the network and the complexity of the dataset. This can also help to understand the relation between local correlations in the input datasets and the performance of the MPO-Nets. More details about this topic can be found in Sec. II C in the SM<sup>51</sup>.

MPOs can be used to represent both fully connected and convolutional layers. In our paper, they are not distinguished from each other at all, and are regarded as the same thing, i.e., linear mappings appeared in Eq. (1). One can also use it just to represent the kernels in convolutional layers, which is a substantially different approach to use MPOs since the convolutional structure is still retained, as suggested by Garipov *et al.*<sup>45</sup>. However, it is more efficient in representing a fully connected layer where the weight matrix is a fully dense matrix. This representation can greatly reduce the memory cost and shorten the training time in a deep neural network where all or most of the linear layers are fully connected ones, such as in a recurrent neural network<sup>46,65,66</sup>, which is used to dispose of video data.

Tensor-network representation of deep neural networks is actually not new. Inspired by the locality assumption about the correlations between pixels, matrix product representation has been already successfully used to characterize and compress images<sup>62</sup>, and to determine the underlying generative models<sup>67</sup>. Novikov *et al.*<sup>37</sup> also used MPOs to represent some

fully connected layers, not including the classifiers, in FC2 and VGG. Our work, however, demonstrates that all fully connected layers, including the classifiers especially, as well as convolutional layers, can be effectively represented by MPOs no matter how deep a neural network is. In other words, in our approach there are no concepts of fully connected layers or convolutional layers, but only linear mappings expressed as sparse MPO and parameter-free non-linear activations. We think this is a great simplification for both concepts and applications, and is of great potential due to the much less required memory space and relatively mathematical structure to study. Our work will greatly help the application of neural networks and especially may help to get rid of connection to the cloud.

There are some previous efforts which aim to establish the entire mapping from the input data to the output label, e.g., Stoudenmire and Schwab tried to represent the mapping in terms of a single MPO<sup>50</sup>. Our proposal differs from it since we are still working in the framework of neural networks, in the sense that the multiple-layer structure and activation functions are still retained. There are also other mathematical structures that have been used to represent deep neural networks due to entanglement consideration from physics. For example, Kosaiifi *et al.*<sup>47</sup> used a Tucker-structure representation, which is a lower-rank approximation of a high-dimensional tensor, to represent a fully connected layer and its input feature. Hallam *et al.*<sup>48</sup> used a tensor network called a multi-scale entangled renormalization ansatz<sup>68</sup> and Liu *et al.*<sup>49</sup> used an unitary tree tensor network<sup>69</sup> to represent the entire mapping from the input to the output labels. Comparing with these works, our approach is a one-dimensional representation which emphasizes more on local entanglement in physics, and it is more efficient and flexible to represent some intermediate layers.

It is valuable to mention two aspects about the MPO representation. One is about its application scope. Due to the locality assumption, it is expected to work efficiently in the data sets where locality can be appropriately defined; otherwise, a large bond dimension would be necessary, which might lead to the loss of efficiency and advantage. The other is about the manner how the input data is ordered when it is fed to the MPO-Net. It is instructive to notice that different orderings of an input vector are related by elementary transformations; therefore, they should lead to the same prediction, in principle, as long as the bond dimension is sufficiently large; while given a small bond dimension, the ordering which keeps better the locality may lead to higher prediction accuracy. A coarse-grained ordering which can better characterize the locality of the original image was proposed in Ref. [62] and is worth

being studied systematically in the future.

In this paper, we have proposed to use MPOs to compress the transformation matrices in deep neural networks. Similar ideas can be used to compress complex data sets, for example, the dataset called ImageNet<sup>59</sup>, in which each image contains about  $224 \times 224$  pixels. In this case, it is matrix product states<sup>70</sup>, instead of MPOs, that should be used. We believe this can reduce the cost in decoding each “image” in a data set, and by combining with the MPO representation of the linear transformation matrices, can further compress deep neural networks and enhance prediction power. A preliminary example is shown in Sec. II E in the SM<sup>51</sup>. Another possible advance in the future is about the analysis of optimization in a neural network. In this work, in most cases, MPO-Nets converge faster than the original networks in the training procedure, and this is probably due to the far fewer parameters. However, in deep learning, due to the strong non-linearity of the cost function, e.g., Eq. (7), more parameters means higher-dimensional variational space and might have more local minima, thus it is difficult for the current optimization approach, e.g., stochastic gradient descent method, to guarantee a faster convergence speed in a model with fewer parameters. The counter-examples can be found in both normal networks and MPO-Nets, as discussed in Sec. II E in the SM<sup>51</sup>. By using MPO representations, as a complementary

tool, we can study this optimization problem in deep learning from the viewpoint of entanglement entropy developed in quantum physics, as we did preliminarily in the SM<sup>51</sup>. Therefore, based on these matrix product representations stemming from quantum many-body physics, it is possible to establish a framework of modern neural networks which might be simpler, cheaper, but more efficient and better understood. It is also expected that this bridge between quantum many-body physics and deep learning can eventually provide some useful feedback and insight to physics, and we would like to leave the extensive study as a future pursuit.

### Acknowledgments

We thank Andrzej Cichocki, Pan Zhang, and Lei Wang for valuable discussions. This work was supported by the National Natural Science Foundation of China (Grants No. 11774420, 11774422, 11874421, 11888101), and by the National R&D Program of China (Grants No. 2016YFA0300503, 2017YFA0302900), and by the Research Funds of Renmin University of China (Grants No. 20XNLG19).

Ze-Feng Gao and Song Cheng contributed equally to this work.

\* qingtaoxie@ruc.edu.cn

† huihai.zhao@riken.jp

‡ zlu@ruc.edu.cn

§ txiang@iphy.ac.cn

- <sup>1</sup> Y. LeCun, B. Boser, J. S. Denker, D. Henderson, R. E. Howard, W. Hubbard, and L. D. Jackel, Backpropagation applied to handwritten zip code recognition, *Neural Comput.* **1**, 541 (1989).
- <sup>2</sup> Y. Lecun, L. Bottou, Y. Bengio, P. Haffner, Gradient-Based Learning Applied to Document Recognition, *Proc. of The IEEE*, **86**, 2278 (1998).
- <sup>3</sup> A. Krizhevsky, I. Sutskever, and G. E. Hinton, ImageNet classification with deep convolutional neural networks, *Advances in NIPS* **25**, 1097 (2012).
- <sup>4</sup> M. Lin, Q. Chen, and S. Yan, Network in network, *ICLR* (2014).
- <sup>5</sup> R. K. Srivastava, K. Greff, and J. Schmidhuber, Training very deep networks, *NIPS* (2015).
- <sup>6</sup> J. Schmidhuber, Deep learning in neural networks: an overview, *Neural Networks*, **61**, 85 (2015).
- <sup>7</sup> G. Larsson, M. Maire, and G. Shakhnarovich, Fractalnet Ultra-deep neural networks without residuals, arXiv:1605.07648.
- <sup>8</sup> C. Szegedy, W. Liu, Y. Jia, P. Sermanet, S. Reed, D. Anguelov, D. Erhan, V. Vanhoucke, and A. Rabinovich, Going deeper with convolutions, *CVPR* (2015), pp.1-9, [https://www.cv-foundation.org/openaccess/content\\_cvpr\\_2015/html/Szegedy\\_Going\\_Deeper\\_With\\_2015\\_CVPR\\_paper.html](https://www.cv-foundation.org/openaccess/content_cvpr_2015/html/Szegedy_Going_Deeper_With_2015_CVPR_paper.html).
- <sup>9</sup> K. Simonyan, A. Zisserman, Very deep convolutional networks for large-scale image recognition, arXiv:1409.1556.
- <sup>10</sup> K. M. He, X. Y. Zhang, S. Q. Ren, J. Sun, Deep residual learning for image recognition, *CVPR* (2016), pp.4700-4708, see [http://openaccess.thecvf.com/content\\_cvpr\\_2016/html/](http://openaccess.thecvf.com/content_cvpr_2016/html/)

[He\\_Deep\\_Residual\\_Learning\\_CVPR\\_2016\\_paper.html](http://openaccess.thecvf.com/content_cvpr_2016/html/He_Deep_Residual_Learning_CVPR_2016_paper.html).

- <sup>11</sup> G. Huang, Z. Liu, L. van der Maaten, K. Q. Weinberger, Densely connected convolutional networks, *CVPR* (2017), [http://openaccess.thecvf.com/content\\_cvpr\\_2017/html/Huang\\_Densely\\_Connected\\_Convolutional\\_CVPR\\_2017\\_paper.html](http://openaccess.thecvf.com/content_cvpr_2017/html/Huang_Densely_Connected_Convolutional_CVPR_2017_paper.html).
- <sup>12</sup> O. Russakovsky, J. Deng, H. Su, J. Krause, S. Satheesh, S. Ma, Z. Huang, A. Karpathy, A. Khosla, M. Bernstein, A. C. Berg, F. F. Li, ImageNet large scale visual recognition challenge, *Int. J. Comput. Vis.*, 115, 211 (2015).
- <sup>13</sup> T. Sainath, A.-R. Mohamed, B. Kingsbury, B. Ramabhadran, Deep convolutional neural networks for LVCSR, in *IEEE International Conference on Acoustics, Speech and Signal Processing* (IEEE, Piscataway, NJ, 2013), pp.8614-8618.
- <sup>14</sup> L. Deng, Y. Liu, Deep learning in natural language processing, (Springer, Singapore, 2018).
- <sup>15</sup> Y. LeCun, Y. Bengio, G. Hinton, Deep learning, *Nature* **521**, 436 (2015).
- <sup>16</sup> G. Hinton, L. Deng, D. Yu, G. E. Dahl, A.-R. Mohamed, N. Jaitly, A. Senior, V. Vanhoucke, P. Nguyen, T. N. Sainath, B. Kingsbury, Deep neural networks for acoustic modeling in speech recognition, *IEEE Signal Processing Magazine* **29**, 82 (2012).
- <sup>17</sup> I. Sutskever, O. Vinyals, Q. V. Le, Sequence to sequence learning with neural networks, *Adv.NIPS* **27**, 3104 (2014).
- <sup>18</sup> H. H. Do, P. Prasad, A. Maag, A. Alsadoon, Deep learning for aspect-based sentiment analysis: a comparative review, *Expert Systems With Applications* **118**, 272 (2019).
- <sup>19</sup> M. Helmstaedter, K. L. Briggman, S. C. Turaga, V. Jain, H. S. Seung, W. Denk/Helmstaedter, Connectomic reconstruction of the inner plexiform layer in the mouse retina, *Nature* **500**, 168 (2013).
- <sup>20</sup> J. Ma, R. P. Sheridan, A. Liaw, G. E. Dahl, V. Svetnik, Deep neural nets as a method for quantitative structure-activity relationships,

- J. Chem. Inf. Model. **55**, 263 (2015).
- 21 P. Baldi, P. Sadowski, D. Whiteson, Searching for exotic particles in high-energy physics with deep learning, *Nat. Commun.* **5**, 4308 (2014).
  - 22 N. Lei, Z. Luo, S. T. Yau, D. X. Gu, Geometric understanding of deep learning, arXiv:1805.10451.
  - 23 N. Lei, K. Su, S. T. Yau, D. X. Gu, A Geometric view of optimal transportation and generative model, *Comput. Aided Geometri Design* **68**, 1 (2019).
  - 24 X. Gao, L. M. Duan, Efficient representation of quantum many-body states with deep neural networks, *Nat. Commun.* **8**, 662 (2017).
  - 25 J. Carrasquilla and R. G. Melko, Machine learning phases of matter, *Nat. Phys.* **13**, 431 (2017).
  - 26 S. H. Li, L. Wang, Neural network renormalization group, *Phys. Rev. Lett.* **121**, 260601 (2018).
  - 27 D. Wu, L. Wang, P. Zhang, Solving statistical mechanics using variational autoregressive networks, *Phys. Rev. Lett.* **122**, 080602 (2019).
  - 28 G. Carleo, I. Cirac, K. Cranmer, L. Daudet, M. Schuld, N. Tishby, L. V.-Maranto, L. Zdeborova, Machine learning and the physical sciences, *Rev. Mod. Phys.* **91**, 045002 (2019).
  - 29 S. Webb, Deep learning for biology, *Nature* **554**, 555 (2018).
  - 30 V. Stanev, C. Oses, A. G. Kusne, E. Rodriguez, J. Paglione, S. Curtarolo, I. Takeuchi, Machine learning modeling of superconducting critical temperature, *npj Comput. Materials* **4**, 29 (2018).
  - 31 K. Hornik, M. Stinchcombe, H. White, Multilayer feedforward networks are universal approximators, *Neural Networks*, **2**, 359 (1989).
  - 32 G. Cybenko, Approximation by superpositions of a sigmoidal function, *Math. Control Signals Systems*, **2**, 303 (1989).
  - 33 P. A. M. Dirac, *The Principles of Quantum Mechanics*, 4th ed. (Clarendon Press, 1982).
  - 34 F. Verstraete, J. J. Garcia-Ripoll, and J. I. Cirac, Matrix product density operators: Simulation of finite-temperature and dissipative systems, *Phys. Rev. Lett.* **93**, 207204 (2004).
  - 35 B. Pirvu, V. Murg, J. I. Cirac and F. Verstraete, Matrix product operator representations, *New J. of Phys.*, **12**, 025012 (2010)
  - 36 I. V. Oseledets, Tensor-Train decomposition, *SIAM J. Scientific Computing*, **33**, 2295 (2011)
  - 37 A. Novikov, D. Podoprikin, A. Osokin, D. Vetrov, Tensorizing neural networks, *Adv. NIPS* **28** 442 (2015).
  - 38 D. Poulin, A. Qarry, R. Somma, F. Verstraete, Quantum simulation of time-Dependent Hamiltonians and the convenient illusion of Hilbert space, *Phys. Rev. Lett.* **106**, 170501 (2011).
  - 39 J. Eisert, M. Cramer, M. B. Plenio, Colloquium: Area laws for the entanglement entropy, *Rev. Mod. Phys.*, **82**, 277 (2010).
  - 40 S. R. White, Density matrix formulation for quantum renormalization groups, *Phys. Rev. Lett.* **69**, 2863 (1992).
  - 41 G. Vidal, Efficient classical simulation of slightly entangled quantum computations, *Phys. Rev. Lett.* **91**, 147902 (2003).
  - 42 M. Denil, B. Shakibi, L. Dinh, M. Ranzato, and N. de Freitas, Predicting parameters in deep learning, *Adv. NIPS* **26**, 2148 (2013)
  - 43 T. N. Sainath, B. Kingsbury, V. Sindhvani, E. Arisoy, and B. Ramabhadran, Low-rank matrix factorization for deep neural network training with high-dimensional output targets, in *IEEE International Conference on Acoustics, Speech and Signal Processing (IEEE, Piscataway, NJ, 2013)*, pp.6655-6659.
  - 44 J. Xue, J. Li, and Y. Gong, Restructuring of deep neural network acoustic models with singular value decomposition, *Interspeech*, 2365 (2013).
  - 45 T. Garipov, D. Podoprikin, A. Novikov, D. Vetrov, Ultimate tensorization: compressing convolutional and fully-connected layers alike, arXiv:1611.03214.
  - 46 Y. Yang, D. Krompass, V. Tresp, Tensor-Train recurrent neural networks for video classification, *ICML* **70**, 3891 (2017).
  - 47 J. Kossaifi, Z. Lipton, A. Khanna, T. Furlanello, A. Anandkumar, Tensor regression networks, arXiv:1707.08308.
  - 48 A. Hallam, E. Grant, V. Stojevic, S. Severini, A. G. Green, Compact neural networks based on the multiscale entanglement renormalization ansatz, arXiv:1711.03357
  - 49 D. Liu, S. J. Ran, P. Wittek, C. Peng, R. B. Garcia, G. Su, and M. Lewenstein, Machine learning by two-dimensional hierarchical tensor networks: A quantum information theoretic perspective on deep architectures, *New J. Phys.* **21**, 073059 (2019).
  - 50 E. Stoudenmire, and D. J. Schwab, Supervised learning with tensor networks, *Adv. NIPS* **29**, 4799 (2016)
  - 51 See Supplemental Material at <http://link.aps.org/supplemental/10.1103/PhysRevResearch.2.023300> for additional information about this work, including the detailed structure of the neural networks used in this work and extra information about the MPO representations.
  - 52 I. Goodfellow, Y. Bengio, A. Courville, *Deep Learning*, (MIT press, 2016).
  - 53 D. E. Rumelhart, G. E. Hinton, R. J. Williams, Nature, Learning representations by back-propagating errors, *Nature*, **323**, 533 (1986)
  - 54 K. P. Murphy, *Machine learning: A probabilistic perspective*, (MIT press, 2012).
  - 55 <https://github.com/zfgao66/deeplearning-mpo>
  - 56 See, e.g., [http://www.tensorfly.cn/tfdoc/tutorials/mnist\\_beginners.html](http://www.tensorfly.cn/tfdoc/tutorials/mnist_beginners.html)
  - 57 The official website of MNIST is available at <http://yann.lecun.com/exdb/mnist>.
  - 58 The official website of CIFAR is available at <https://www.cs.toronto.edu/~kriz/cifar.html>.
  - 59 The official website of ImageNet is available at <http://www.image-net.org>
  - 60 See, e.g., <http://www.worldlink.com.cn/en/osdir/fashion-mnist.html>
  - 61 The official website of SVHN is available at <http://ufldl.stanford.edu/housenumbers/>
  - 62 J. I. Latorre, Image compression and entanglement, arXiv:quant-ph/0510031.
  - 63 Some numerical analysis on the MNIST dataset based on the entropy calculation has been devoted to topic. E.g., see Song Cheng, Jing Chen, and Lei Wang, Information perspective to probabilistic modeling: Boltzmann machines versus Born machines, *Entropy*, **20**, 583 (2018)
  - 64 D. Perez-Garcia, F. Verstraete, M. M. Wolf, J. I. Cirac, Matrix product state representations, *Quantum Inf. Comput.* **7**, 401 (2007)
  - 65 S. Hochreiter, J. Schmidhuber, Long short-term memory, *Neural Comput.* **9**, 1735 (1997)
  - 66 C. Guo, Z. Jie, W. Lu, D. Poletti, Matrix product operators for sequence-to-sequence learning, *Phys. Rev. E* **98**, 042114 (2018)
  - 67 Z. Y. Han, J. Wang, H. Fan, L. Wang, P. Zhang, Unsupervised generative modeling using matrix product states, *Phys. Rev. X* **8**, 031012 (2018)
  - 68 G. Vidal, Entanglement renormalization, *Phys. Rev. Lett.*, **99**, 220405 (2007)
  - 69 Y. Shi, L. M. Duan, and G. Vidal, Classical simulation of quantum many-body systems with a tree tensor network, *Phys. Rev. A*, **74**, 022320 (2006)
  - 70 M. Fannes, B. Nachtergaele, Finitely correlated states on quantum spin chains, *Comm. Math. Phys.*, **144**, 443 (1992)



## Supplemental Materials: Compressing deep neural networks by matrix product operators

In this supplemental material, we give the detailed structure of the neural networks used in this work, and provide extra information about the MPO representation, such as performance on more datasets, different factorization manners, entanglement entropy grasped, the influence of L2 regularization, convergence of training, and so on. These materials will help to understand our work better. The corresponding source code used in this work is available at <https://github.com/zfgao66/deeplearning-mpo>.

### Section I. Structure Details of the Neural Networks

The used structures of FC2, LeNet5, VGG, ResNet, DenseNet in this paper are summarized in Tab. II-VII, and their prototypes can be found in Ref. <sup>2,9-11,56</sup>, respectively. In order to simplify the descriptions, firstly we introduce some short-hands summarized in Tab. I which are used in this materials.

Abbreviation	Meaning
MaxPo	a max-pooling layer
AvgPo	an average-pooling layer
Conv	a convolutional layer
ConvUnit	a unit composed of convolutional layers
ResUnit	a unit introduced in ResNet
ResBlock	a block composed of several ResUnits
DenseUnit	a unit introduced in DenseNet
BN	batch normalization
$[w, h; c; s]$	a convolutional layer with $c$ kernels each with width $w$ height $h$ and stride $s$
$[w, h; s]$	a pooling layer with pooling width $w$ height $h$ and stride $s$
$\{w, h; c; s, t\}$	a ResUnit composed of two convolutional layers denoted as width $\{w, h; c; s\}$ and $\{w, h; c; t\}$ resp.
$N_{para}$	number of parameters in the linear layers
Represented	whether this block of layers are represented by MPO in the preliminary test

TABLE I. The short-hands used in this materials.

No.	Layer name	Input size	Output size	Comment	$N_{para}$	Represented
1	FC	28×28	256		200704	Yes
				ReLU		
2	FC	256	10		2560	Yes
				Softmax		

TABLE II. The FC2 network structure used in this work. ReLu and Softmax are element-wise operations, whose details are not shown here and after.

No.	Layer name	Input size	Output size	Comment	$N_{para}$	Represented
1	Conv	28×28	28×28×6	[5,5;6;1]	150	
	ReLu					
	MaxPo	28×28×6	14×14×6	[2,2;2]		
2	Conv	14×14×6	10×10×16	[5, 5; 16; 1] <sub>np</sub>	2400	
	ReLu					
	MaxPo	10×10×16	5×5×16	[2,2;2]		
3	Conv	5×5×16	120	[5, 5; 120; 1] <sub>np</sub>	48000	Yes
	ReLu					
4	FC	120	84		10080	Yes
	ReLu					
5	FC	84	10		840	Yes
	Softmax					

TABLE III. The LeNet5 network structure used in this work. Here the subscript  $np$  is used to emphasize that no padding is used in convolutions there.

No.	Layer name	Input size	Output size	Comment	$N_{para}$	Represented
1	ConvUnit	32×32×3	32×32×64	2×[3,3;64;1]	38592	
	ReLu					
	MaxPo	32×32×64	16×16×64	[2,2;2]		
2	ConvUnit	16×16×64	16×16×128	2×[3,3;128;1]	221184	
	ReLu					
	MaxPo	16×16×128	8×8×128	[2,2;2]		
3	ConvUnit	8×8×128	8×8×256	2×[3,3;256;1]	884736	
	ReLu					
4	Conv	8×8×256	8×8×256	[1,1;256;1]	65536	
	ReLu					
	MaxPo	8×8×256	4×4×256	[2,2;2]		
5	ConvUnit	4×4×256	4×4×512	2×[3,3;512;1]	3538944	
	ReLu					
6	Conv	4×4×512	4×4×512	[1,1;512;1]	262144	
	ReLu					
	MaxPo	4×4×512	2×2×512	[2,2;2]		
7	ConvUnit	2×2×512	2×2×512	2×[3,3;512;1]	4718592	Yes
	ReLu					
8	Conv	2×2×512	2×2×512	[1,1;512;1]	262144	
	ReLu					
	MaxPo	2×2×512	512	[2,2;2]		
9	FC	512	4096		2097152	Yes
	ReLu					
10	FC	4096	4096		16777216	Yes
	ReLu					
11	FC	4096	10		40960	Yes
	Softmax					

TABLE IV. The VGG-16 network structure used in this work. Here a ConvUnit denoted with  $m\times$  means  $m$  convolutional layers separated by ReLu.

No.	Layer name	Input size	Output size	Comment	$N_{para}$	Represented
1	ConvUnit	32×32×3	32×32×64	2×[3,3;64;1]	38592	
				ReLu		
	MaxPo	32×32×64	16×16×64	[2,2;2]		
2	ConvUnit	16×16×64	16×16×128	2×[3,3;128;1]	221184	
				ReLu		
	MaxPo	16×16×128	8×8×128	[2,2;2]		
3	ConvUnit	8×8×128	8×8×256	4×[3,3;256;1]	2064384	
				ReLu		
	MaxPo	8×8×256	4×4×256	[2,2;2]		
4	ConvUnit	4×4×256	4×4×512	4×[3,3;512;1]	8257536	
				ReLu		
	MaxPo	4×4×512	2×2×512	[2,2;2]		
5	ConvUnit	2×2×512	2×2×512	4×[3,3;512;1]	9437184	Partially
				ReLu		
	MaxPo	2×2×512	512	[2,2;2]		
6	FC	512	4096		2097152	Yes
				ReLu		
7	FC	4096	4096		16777216	Yes
				ReLu		
8	FC	4096	10		40960	Yes
				Softmax		

TABLE V. The VGG-19 network structure used in this work. Here a ConvUnit denoted with  $m\times$  means  $m$  convolutional layers separated by ReLu. By *partially* we mean the last two convolutional layers in that ConvUnit was represented by MPO.

No.	Layer name	Input size	Output size	Comment	$N_{para}$	Represented
1	Conv	32×32×3	32×32×16	[3,3;16;1]	432	
				BN + ReLu		
2	ResBlock	32×32×16	32×32×16k	$m\times\{3, 3; 16k; 1, 1\}$	$2304k[(2m - 1)k + 1]$	
				BN + ReLu		
3	ResUnit	32×32×16k	16×16×32k	{3, 3; 32k; 2, 1}	$13824k$	
				BN + ReLu		
4	ResBlock	16×16×32k	16×16×32k	$(m-1)\times\{3, 3; 32k; 1, 1\}$	$18432k^2(m - 1)$	
				BN + ReLu		
5	ResUnit	16×16×32k	8×8×64k	{3, 3; 64k; 2, 1}	$55296k$	
				BN + ReLu		
5	ResBlock	8×8×64k	8×8×64k	$(m-1)\times\{3, 3; 64k; 1, 1\}$	$73728k^2(m - 1)$	Partially
				BN + ReLu		
	AvgPo	8×8×64k	64k	[8,8;8]		
6	FC	64k	10		640k	Yes
				Softmax		

TABLE VI. The ResNet network structure used in this work. The total depth  $L$  is given by  $L = 6m + 2$ . Here in a single ResUnit, the two convolutional layers are separated by batch normalization and ReLu, and a ResBlock denoted with  $m\times$  means  $m$  ResUnits separated by batch normalization and ReLu. By *Partially* we mean the last ResUnit in that ResBlock is represented by MPO.

Dataset	Network	Original Rep	MPO-Net	
		$a$ (%)	$a$ (%)	$\rho$
Fashion-MNIST	VGG-16	94.96	94.88	$\sim 0.0005$
	VGG-19	95.07	94.95	$\sim 0.0005$
SVHN	VGG-16	96.166	96.331	$\sim 0.0005$
	VGG-19	96.266	96.412	$\sim 0.0005$
	DenseNet	96.354	96.235	$\sim 0.129$

TABLE VIII. Test accuracy  $a$  and compression ratios  $\rho$  obtained in the original and MPO representations in VGG and DenseNet. **Note:** in this table, the standard deviations ( $\sigma$ ) of VGG16, VGG19 and DenseNet are about 0.4%, 0.2%, 0.2%, respectively, while the standard deviations ( $\sigma$ ) of all relative MPO-nets are about 0.1%. Therefore, the results from normal networks and the MPO counterparts are consistent essentially.

No.	Layer name	Input size	Output size	Comment	$N_{para}$	Represented
1	Conv	$32 \times 32 \times 3$	$32 \times 32 \times n$	[3,3;n;1]	$27n$	
BN + ReLu						
2	DenseUnit	$32 \times 32 \times n$	$32 \times 32 \times (n+km)$	$m \times [3,3;k;1]$	$9km[n + k(m-1)/2]$	
BN + ReLu						
3	Conv	$32 \times 32 \times (n+km)$	$32 \times 32 \times (n+km)$	[1,1;n+km;1]	$(n+km)^2$	
	AvgPo	$32 \times 32 \times (n+km)$	$16 \times 16 \times (n+km)$	[2,2;2]		
BN + ReLu						
4	DenseUnit	$16 \times 16 \times (n+km)$	$16 \times 16 \times (n+2km)$	$m \times [3,3;k;1]$	$9km[n + km + k(m-1)/2]$	
BN + ReLu						
5	Conv	$16 \times 16 \times (n+2km)$	$16 \times 16 \times (n+2km)$	[1,1;n+2km;1]	$(n+2km)^2$	
	AvgPo	$16 \times 16 \times (n+2km)$	$8 \times 8 \times (n+2km)$	[2,2;2]		
BN + ReLu						
6	DenseUnit	$8 \times 8 \times (n+2km)$	$8 \times 8 \times (n+3km)$	$m \times [3,3;k;1]$	$9km[n + 2km + k(m-1)/2]$	Partially
	BN + ReLu					
	AvgPo	$8 \times 8 \times (n+3km)$	$n+3km$	[8,8;8]		
7	FC	$n+3km$	10		$10(n+3km)$	Yes
Softmax						

TABLE VII. The DenseNet network structure used in this work. The total depth  $L$  is given by  $L = 3m + 4$ . A DenseUnit denoted with  $m \times$  means there are  $m$  convolutional layers separated by batch normalization and ReLu in this unit. By *Partially* we mean the last convolutional layer there is represented by MPO.

## Section II. Extra information about MPO-Net

### A. Performance on more datasets

In order to show the validity of the MPO representation further, we have also applied it to another two more sophisticated datasets than MNIST, i.e., the Fashion-MNIST<sup>60</sup> and the Street View House Number (SVHN)<sup>61</sup>.

The Fashion-MNIST consists of a training set of 60,000 examples and a test set of 10,000 examples. Each image is a square of  $28 \times 28$  grayscale pixels, and all the images are divided into 10 classes corresponding to T-shirt, trousers, pullover, dress, coat, sandal, shirt, sneaker, bag, and ankle boot, respectively. We have tested MPO representations in VGG-16, VGG-19, and the ResNet. The detailed structures are already listed in Tab. IV, V, and VI. As shown in Fig. 1, with depth up to 50, the MPO can indeed faithfully represent the linear transformations in the ResNet. And the performance in VGG network is shown in Tab. VIII, which also evidences the validity of MPO in both VGG-16 and VGG-19.

For the SVHN dataset, it consists of a training set of 73,257 examples and a test set of 26,032 examples. Each image is a square of  $32 \times 32$  RGB pixels coming from significantly harder, unsolved, real world problem (recognizing digits and numbers in natural scene images), and all the images are divided into 10 classes corresponding to numbers 0~9, respectively. We have tested MPO representations in the VGG-16, VGG-19, ResNet, and the DenseNet. The detailed structures are listed in Tab. IV, V, VI, and VII. The results are summarized in Fig. 2 and Tab. VIII. The conclusion is the same as in the case of Fashion-MNIST,

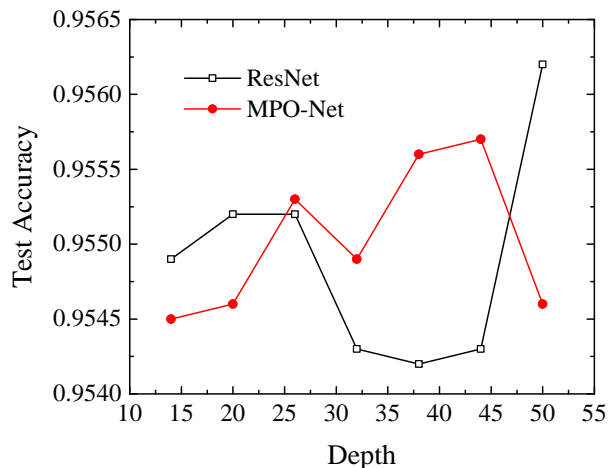


FIG. 1. Comparison of the test accuracy  $a$  between the original and MPO representations of ResNet on Fashion-MNIST with  $k = 4$ . The compression ratio of MPO-Net  $\rho \sim 0.11$ . **Note:** in this plot, the standard deviations ( $\sigma$ ) of ResNet and MPO-Net are about 0.002 and 0.001, respectively, therefore, the two lines can be regarded as very consistent at all depths.

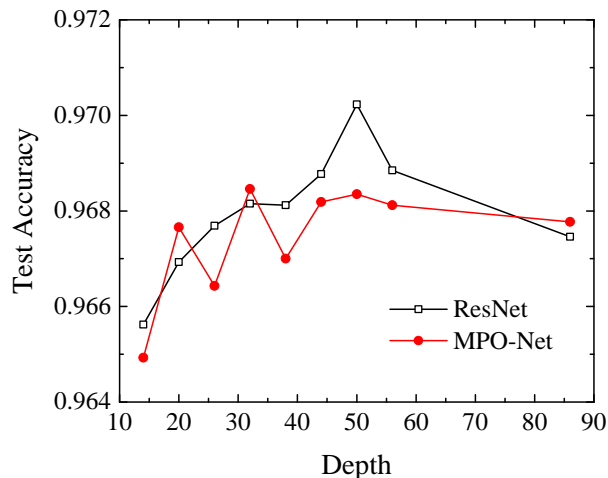


FIG. 2. Comparison of the test accuracy  $a$  between the original and the MPO representations of ResNet on SVHN with  $k = 4$ . The compression ratio of MPO-Net  $\rho \sim 0.11$ . **Note:** in this plot, the standard deviations ( $\sigma$ ) of ResNet and MPO-Net are about 0.002 and 0.001, respectively, therefore, the two lines can be regarded as very consistent at all depths.

i.e., MPO can work well in these networks.

It is definitely impossible to exhaust all the existing datasets and neural networks, but the validity in the five networks, i.e., FC2, LeNet-5, VGG-16(19), ResNet, and DenseNet, on the four datasets, i.e., MNIST, CIFAR-10, Fashion-MNIST, and SVHN, should have provided a strong evidence that MPO can indeed represent the linear transformations faithfully, especially the fully-connected layers and heaviest convolutional layers, in a general deep neural networks.

## B. Factorization manner

As claimed in the main text, the factorization manner of the hidden neurons, i.e., how the  $N_x$  and  $N_y$  are decomposed into  $I_k$  and  $J_k$  in Eq.(4), is chosen by convenience due to fact that testing all possible decompositions is very time-consuming. In the viewpoint of optimization, different factorization manners affect directly the number of variational parameters, thus will definitely affect the test accuracy. However, in the viewpoint of entanglement entropy, that is controlled by the bond dimension  $D$ , as  $D$  becomes larger, the entanglement entropy of the input data grasped by MPO grows accordingly and the accuracy is expected to be improved, thus  $D$  will be more important as long as the network is away from underfitting. In other word, when  $D$  becomes larger, different factorization manner should not make too much differences.

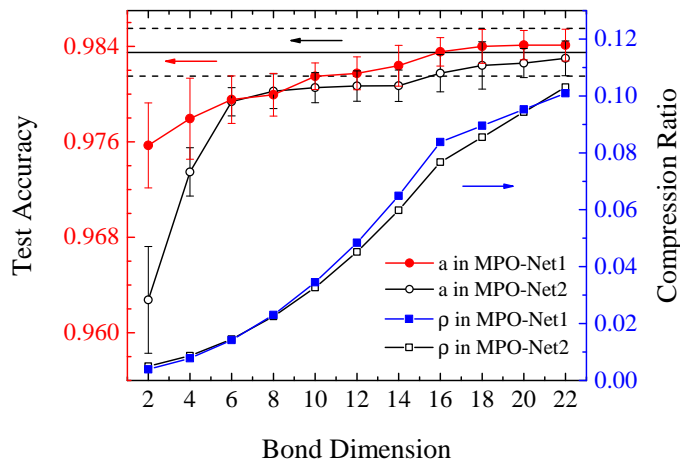


FIG. 3. Comparison of the test accuracy on MNIST dataset between two different MPO-Nets. The two MPO-Nets are differed by using different factorization manners of the fully-connected layers in the same FC2 structure. The solid straight line denotes the test accuracy obtained by the normal FC2,  $98.35\% \pm 0.2\%$ , and the dashed straight lines are also plotted to indicate its error bar.

Dataset	Network	MPO-Net1		MPO-Net2	
		$a$ (%)	$\rho$	$a$ (%)	$\rho$
CIFAR-10	VGG-19	$93.80 \pm 0.09$	0.0005	93.78	0.0006

TABLE IX. Comparison of the test accuracy on CIFAR-10 dataset between two different MPO-Nets. The two MPO-Nets are differed by using different factorization manners of the three fully-connected layers in the same VGG-19 structure. Due to limited resources, MPO-Net2 has been run 1 time only, but the result is already consistent with that obtained from MPO-Net1.

We verified this argument in two experiments. One is the FC2 network on MNIST dataset, the other is the VGG-19 network on CIFAR-10 dataset. In both cases, MPO-Net1 is the network we used in the main text, whose details is listed either in Tab. II and Tab. V. As to the FC2 network, the result is shown in Fig. 3, where MPO-Net2 uses  $M_{2,2,4,4,2,2}^{2,2,4,4,2,2}(D)$  and  $M_{2,2,7,7,2,2}^{1,1,2,5,1,1}(D)$  to represent the two fully-connected layers there. It shows clearly that when  $D \geq 4$ , the two MPO-Nets produce the same test accuracy essentially, and both of them can reproduce the FC2 result. For the VGG-19 network, the result is shown in Tab. IX, where MPO-Net2 uses  $M_{2,8,8,8,2}^{2,8,8,8,2}(4)$ ,  $M_{2,8,8,8,2}^{2,8,8,8,2}(4)$ ,  $M_{2,4,8,4,2}^{2,8,8,8,4}(4)$ ,  $M_{2,8,8,8,4}^{2,8,8,8,4}(4)$  and  $M_{2,8,8,8,4}^{1,10,1,1,1}(4)$  to represent the last five heaviest linear transformations. The obtained accuracy of the two MPO-Nets are identical within the error bar, and both of them coincide with, and a little better than, the normal VGG-19 result,  $93.36\% \pm 0.09\%$ .

In both cases, the obtained results support our argument above, i.e., when  $D$  becomes larger, different factorization manners produce almost the same result.

### C. Entanglement entropy

Since entanglement entropy is only defined for a quantum state, there is no widely-accepted approach to measure the entanglement entropy of a set of classical configurations, e.g., image pixels in a dataset. Nevertheless, in MPO-Nets, it is possible to use the entanglement spectra of the obtained MPO from training to define an entanglement entropy, which can be regarded as an approximated characterization of the entanglement entropy hidden in the underlying input dataset. Since in quantum physics, entanglement entropy is obtained by bipartition of the full system, it can be argued that the larger the entanglement entropy is, the less local the entanglement or correlation in the dataset is, and vice versa. In this section, we use this approach to compare the entanglement entropy between MNIST and Fashion-MNIST.

To be specific, to simplify the idea we train the MPO-Net counterpart of the FC2 network on the two datasets respectively, and then use the first MPO in the networks to obtain the entropy. In our calculation, the first MPO in both cases,  $M_{4,7,7,4}^{4,4,4,4}$ , can be illustrated as in Fig. 4. After training, all the four local tensors are known, and we can obtain the normalized entanglement spectra by either obtaining the canonical form<sup>64</sup> of the MPO representation or decomposing the corresponding matrix through singular value decomposition. E.g., for bond1 in Fig. 4, we can fuse the indices to form a matrix  $T_{i_1 j_1, i_2 i_3 i_4 j_2 j_3 j_4}$  and obtain its

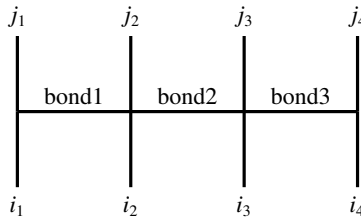


FIG. 4. MPO configuration,  $M_{4,7,7,4}^{4,4,4,4}$ , used in the calculation of entanglement entropy. As listed in Tab. II and in the main text, all the dimensions  $I$ s and  $J$ s are 4, except  $I_2 = I_3 = 7$  due to the input size is  $28 \times 28$ .

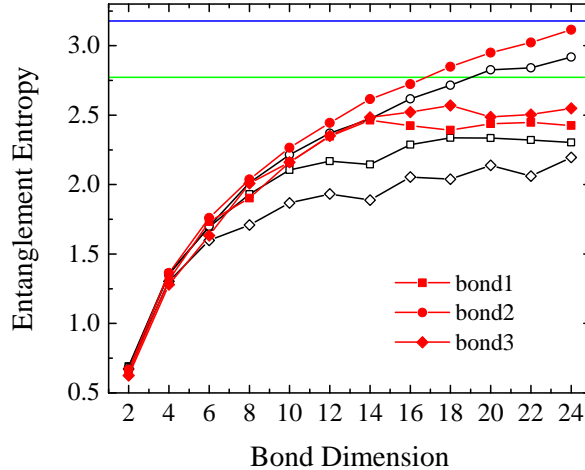


FIG. 5. Entanglement entropy measured from three bonds as shown in Fig. 4 and obtained from the first MPO in the two FC2-MPO networks after well-trained on the MNIST (black curves) and Fashion-MNIST (red curves) datasets. The two straight lines are the theoretical upper bounds of the entropies that the MPO-Net could grasp, i.e., blue line is  $\ln 24$  for bond2, and green line is  $\ln 16$  for bond1 and bond3.

singular values  $v_i$ , then the entanglement spectra  $\lambda$  and entanglement entropy  $S$  can be obtained in the following

$$S = - \sum_i \lambda_i \ln \lambda_i, \quad \text{where} \quad \lambda_i = \frac{v_i^2}{\sum v_i^2} \quad (1)$$

The entropy measured from bond2 and bond3 can be obtained similarly.

The result is summarized in Fig. 5. It shows that for all the three bonds, the entanglement entropy obtained from Fashion-MNIST is generally larger than that obtained from MNIST, especially the entropy on bond2 from Fashion-MNIST almost saturates to the upper bound when  $D = 24$ . This probably means that the correlation in MNIST is much more local than Fashion-MNIST, which is consistent with the fact that FC2 and its MPO-Net counterpart can work much better in MNIST, while for Fashion-MNIST, to obtain a comparative accuracy, one has to use more complicated network, e.g., VGG and ResNet, as shown in Fig. 1 and Tab. VIII, or their MPO-Net counterparts. This example shows that MPO-Net, as well as its normal counterpart, indeed perform better in the systems where local entanglement or correlation plays an important role, while for the systems where most of the correlation is long-range, they probably perform worse. In fact, in our construction, for the Fashion-MNIST data, FC2 and LeNet-5, and their MPO-Net counterparts, can only give a test accuracy about 90%, much lower than that in MNIST.

By the way, it seems also in Fig. 5 that the entropy converges to a rather lower value than the theoretical limit on the 1st and 3rd bond for both two datasets, and this actually addresses the existence of locality in the MNIST and Fashion-MNIST datasets, and provides the possibility to apply MPO-Nets on these datasets (but with more layers probably).

#### D. About L2 regularization

Essentially, L2 regularization can be regarded as a constrain on the variational parameters in the neural networks. In the field of deep learning, it is believed to be able to alleviate overfitting, and is widely used in modern neural networks<sup>52</sup>. Therefore, in all the networks mentioned in this work, including both the normal neural networks, such as FC2, LeNet-5, VGG, ResNet,

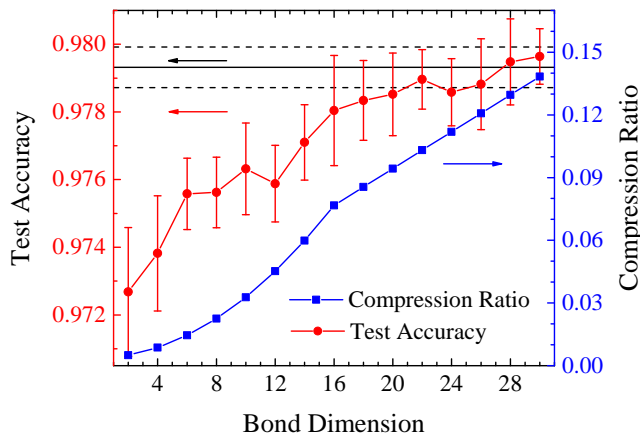


FIG. 6. Comparison of the test accuracy  $a$  between the FC2 and the corresponding MPO-Net on MNIST dataset, without L2 regularization. The corresponding compression ratio  $\rho$  is also plotted for each bond dimension  $D$ .

Dataset	Network	Original Rep.	MPO-Net	
		$a$ (%)	$a$ (%)	$\rho$
CIFAR-10	VGG-16	92.39	92.90	0.0005
CIFAR-10	VGG-19	92.48	92.91	0.0005

TABLE X. Comparison of the test accuracy obtained between VGG networks and the corresponding MPO-Nets. None of the networks here uses L2 regularization.

and DenseNet, as well as the corresponding MPO-Net counterparts, the L2 regularization is always used. However, the validity of MPO representation does not rely on the usage of regularization, i.e., without L2 regularization, MPO-Net should still work well. In this section, we redo the comparison in Fig.2 and Table.1 in the main text, i.e., performance comparison between MPO-Net and normal networks on MNIST, to verify this statement, but without L2 regularization.

In Fig. 6, the comparison between FC2 and the corresponding MPO-Net on MNIST is shown. It can be seen clearly that though both the two results are little worse than the results obtained with L2 normalization, the MPO-Net can still reproduce the FC2 results when  $D$  becomes large, e.g.,  $D \geq 16$ . Similar conclusion can be drawn from Tab. X, in which the comparison between VGG networks and the corresponding MPO-Nets on CIFAR-10 is shown, i.e., under such situations, the MPO-Nets can still work at least equally well with normal VGG networks. Thus, we could conclude that the validity of the MPO-Nets is irrelevant to the L2 regularization.

### E. Convergence of training

One of the motivations of using MPO to represent the linear transformations in deep neural networks is that, with fewer parameters, the training can be expected much easier to converge. However, due to the strong nonlinearity of the cost function, as expressed in Eq. (7) in the main text, more parameters means higher-dimensional variational space and might have more local minima, thus it is difficult for the current optimization approach, e.g., stochastic gradient descent method, to guarantee a faster convergence speed in a model with fewer parameters. This can be seen from the several networks we used in this paper. E.g., as listed in Tab. XI, FC2 has more parameters than LeNet-5, but it converges faster, while the DenseNet has much fewer parameters than VGG-19 and ResNet, however, it needs more epoches to converge the training accuracy.

Things are more complicated in the case of MPO-Nets. More study shows that it is also related the fact that how much relevant entanglement is hidden in the input data and how much entanglement is grasped by the MPO-Nets. To show this, in Fig. 7, we plot the training procedures for FC2 and the corresponding MPO-Nets on MNIST dataset. As done in Ref. <sup>62</sup>, similarly we can represent the input images in terms of matrix product states (MPS)<sup>70</sup>, and as proposed in the discussion section in the main text, then we can combine the MPS representation of the iamges and the MPO-Nets together to form a complete new network. Suppose the bond dimension of the MPS is denoted as  $\chi$ , then we know in quantum physics that  $\chi$  controls the maximal entanglement grasped in the MPS representation. For MNIST, each image is a  $28 \times 28$  square matrix, thus the maximal meaningful  $\chi$  is 28, which corresponds to the original image, as shown in (c) in Fig. 7. We can also throw some irrelevant information by truncating the MPS and use a smaller bond dimension  $\chi$  for the input data, as shown in (a) and (b) in Fig. 7. In



DataSet	Network	Total parameters	Necessary epoches for training
MNIST	FC2	203,264	~ 25
	LeNet-5	61,470	~ 40
CIFAR-10	VGG-19	38,934,208	~ 150
	ResNet (k=4, m=18)	26,646,448	~ 150
	DenseNet (n=16, k=m=12)	1,001,616	~ 300

TABLE XI. Extra information about some normal networks used in this work, including the total parameters in the networks and the necessary epoches for the training procedure.

all the three cases, we have compared the convergence behavior of the training procedures among two different MPO-Nets and the original FC2 network.

It shows that, when  $\chi$  is small, e.g.  $\chi = 2$ , there is very little entanglement in the input data, the MPO-Net with  $D = 2$  is underfitting and converges much slowly, while MPO-Net with  $D = 16$  can produce a higher training accuracy at the same training steps and eventually converges to accuracy 100% after more epoches than FC2. As  $\chi$  becomes larger, e.g.,  $\chi = 10$  and the original data ( $\chi = 28$ ), there is more entanglement represented in the input data, the MPO-Net with  $D = 2$  is still some kind of underfitting and converges slowly, while MPO-Net with  $D = 16$  can indeed converge much faster than the original FC2 and obtain a higher accuracy at the same training step. Therefore, as to the MPO-Nets, although in most cases they usually converge faster than the original network, it is difficult to guarantee a faster convergence for the training due to the complicated nonlinear structure of the cost function, the convergence behavior of the optimization methods, as shown in Tab. XI, the entanglement entropy hidden in the input data, and the grasped entanglement entropy in the MPO representations, as shown in Fig. 7. This provides the possibility of analyzing the long-standing unsolved optimization problems in deep learning by entanglement entropy developed in quantum physics. A complete understanding of the exact relationship can probably improve the current learning algorithm, which will be a pursuit in the future work.

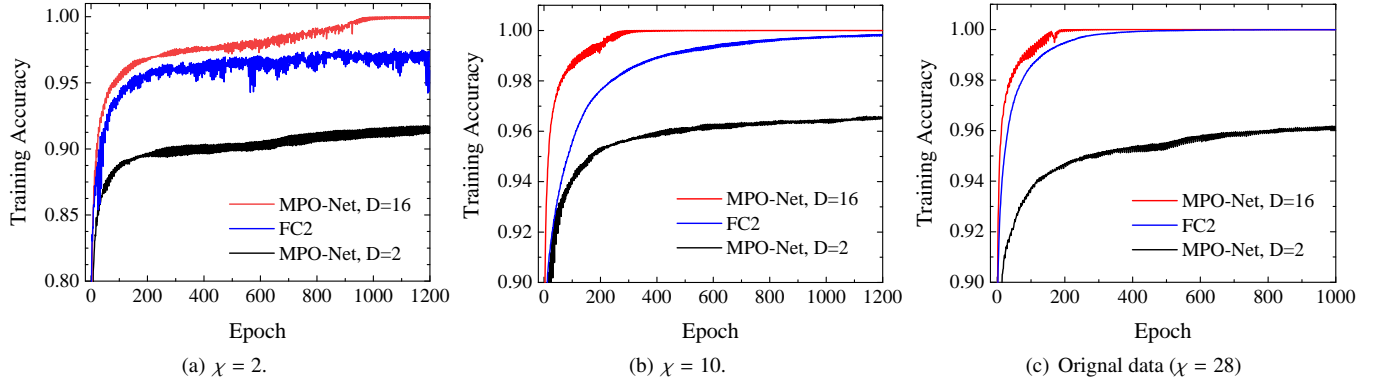


FIG. 7. Comparison of the train accuracy obtained between FC2 and MPO-Nets on MNIST, with different representations of the input data on MNIST. Parameter  $\chi$  is used to truncate the MPS and to control the entanglement entropy embodied in the representation.